The Transcription Factor Gene *Nfib* Is Essential for both Lung Maturation and Brain Development

George Steele-Perkins,[1]† Céline Plachez,[2] Kenneth G. Butz,[1] Guanhu Yang,[3]
Cindy J. Bachurski,[3] Stephen L. Kinsman,[4] E. David Litwack,[2]
Linda J. Richards,[2] and Richard M. Gronostajski[1]*

*Department of Biochemistry and the Program in Neuroscience, State University of New York at Buffalo, Buffalo,
New York[1]; Division of Pulmonary Biology, Cincinnati Children's Research Foundation, Cincinnati, Ohio[3];
and Department of Anatomy and Neurobiology and Program in Neuroscience[2] and Department
of Pediatrics,[4] University of Maryland, Baltimore, School of Medicine,
Baltimore, Maryland*

The phylogenetically conserved nuclear factor I (NFI) gene family encodes site-specific transcription factors essential for the development of a number of organ systems. We showed previously that *Nfia*-deficient mice exhibit agenesis of the corpus callosum and other forebrain defects, whereas *Nfic*-deficient mice have agenesis of molar tooth roots and severe incisor defects. Here we show that *Nfib*-deficient mice possess unique defects in lung maturation and exhibit callosal agenesis and forebrain defects that are similar to, but more severe than, those seen in *Nfia*-deficient animals. In addition, loss of *Nfib* results in defects in basilar pons formation and hippocampus development that are not seen in *Nfia*-deficient mice. Heterozygous *Nfib*-deficient animals also exhibit callosal agenesis and delayed lung maturation, indicating haploinsufficiency at the *Nfib* locus. The similarity in brain defects in *Nfia*- and *Nfib*-deficient animals suggests that these two genes may cooperate in late fetal forebrain development, while *Nfib* is essential for late fetal lung maturation and development of the pons.

Nuclear factor I (NFI) transcription and replication proteins function both in adenoviral DNA replication (12, 43, 44) and in the regulation of transcription throughout development (21). There are four NFI genes in mammals (*Nfia*, *Nfib*, *Nfic*, and *Nfix*) and single NFI genes in *Drosophila melanogaster*, *Caenorhabditis elegans*, *Anopheles* spp., and other simple animals (21, 30, 50). No NFI genes have been found in plants, bacteria, or single-cell eukaryotes. In mammals, NFI proteins function as homo- or heterodimers and are expressed in complex, overlapping patterns during embryogenesis (6, 31). NFI proteins bind to a dyad-symmetric binding site (TTGGCN₅GCCAA) with high affinity (20, 40), and NFI proteins have been shown to either activate or repress gene expression depending on the promoter and cellular context (21, 42). The presence of four NFI genes in mammals with possibly overlapping functions makes it a challenge to identify in vivo targets of individual NFI proteins and the roles of NFI genes in development.

We showed previously that disruption of *Nfia* causes late gestation neuroanatomical defects, including agenesis of the corpus callosum, size reductions in other forebrain commissures, and loss of specific midline glial populations (11, 56). In contrast, disruption of *Nfic* results in early postnatal defects in tooth formation, including the loss of molar roots and aberrant incisor development (61). In a previous study, insertion of a *lacZ* reporter gene into the *Nfib* locus resulted in defects in

lung maturation but no apparent defects in brain development (22). Here we report the replacement of the essential exon 2 of the *Nfib* gene with a *lacZ* reporter gene and show that mice homozygous for our replacement mutation have major neuroanatomical defects similar to, but more severe than, those of *Nfia*⁻/⁻ mice. These defects include callosal agenesis, aberrant hippocampus and pons formation, and loss of specific midline glial populations. In addition, as was seen in the previously described *Nfib* insertion mutant, these *Nfib*-deficient animals show defects in lung development and die at birth with immature lungs. The loss of one copy of *Nfib* results in callosal agenesis in some animals and reduced lung maturation in all animals, demonstrating haploinsufficiency at the *Nfib* locus. Together, these defects indicate that *Nfia* and *Nfib* may function cooperatively during mouse forebrain development and that *Nfib* alone is essential for late gestational lung maturation and hippocampus and pons development.

MATERIALS AND METHODS

Gene targeting and mouse strains. Genomic clones containing *Nfib* exons 1 and 2 were isolated from a mouse 129/Sv phage library as described previously (11, 61). We modified *lacZ* to encode the simian virus 40 T antigen nuclear localization signal (NLS) at the β-galactosidase (β-Gal) N terminus and to include a phosphoglycerate kinase (PGK) gene poly(A) signal at its 3′ end (64), generating NLS–β-Gal–pA. Using a convenient EcoRI site at the 5′ end of exon 2 we cloned NLS–β-Gal–pA in frame with a 5.65-kb *Nfib* fragment ending at base 9 of exon 2 to form a translational fusion protein with the product of exon 2 of *Nfib*. A PGK-Neo-bGHpA cassette (60) was cloned downstream of the *lacZ* fusion cassette, followed by ~3 kb of intron 2. The NLS–β-Gal–pA and Neo cassettes replace 700 bp of *Nfib*, including all but 9 bp of exon 2. A diphtheria toxin A chain-expressing negative selection cassette (PGK-DTA-bGHpA) was assembled and cloned downstream of the 3′ homologous region in the opposite transcriptional orientation (67). E14-1 mouse embryonic stem (ES) cells (5 ×

* Corresponding author. Mailing address: State University of New York at Buffalo, Dept. of Biochemistry, 140 Farber Hall, 3435 Main St., Buffalo, NY 14214-3000. Phone: (716) 829-3471. Fax: (716) 829-2725. E-mail: rgron@buffalo.edu.
† Present address: Buffalo, NY 14215.

10^6) were electroporated with 5 μg of gel-purified 15.2-kb XhoI targeting vector fragment and then selected in 0.2-mg/ml G418 (GIBCO/BRL) for 6 days. Colonies were picked and expanded twice in 96-well plates. Two plates were frozen, and two were used for DNA isolation and Southern blot analyses.

Correctly targeted ES cells were injected into C57BL/6 blastocysts, and stable transmission of the targeted allele was assessed by PCR genotyping of the progeny of founder male chimeras. The targeted (knockout [KO]) allele was crossed into Black Swiss (Taconic), C57BL/6 (Taconic and Jackson Laboratories), and FVB/N (Jackson Laboratories) strains for analysis. Mice derived from two independent targeted ES cell clones were analyzed and had indistinguishable phenotypes. Since some 129 strains of mice have a recessive callosal agenesis phenotype (35, 36) and since the ES cells used were derived from 129S6 mice, all brain sections were prepared from mice backcrossed into the Black Swiss (one generation) or C57BL/6 (more than five generations) strain to avoid the as yet uncharacterized 129 recessive acallosal-susceptibility locus. The lung morphology phenotypes of *Nfib* mutant animals of the Black Swiss, C57BL/6, and FVB/N strains were indistinguishable. Each figure legend contains the strain used in the figure.

PCR genotyping. Postnatal day 10 (P10) to P14 0.5-cm tail tip biopsy samples were shaken at 55°C overnight in 0.5 ml of tail lysis buffer (100 mM Tris-Cl [pH 8.5], 5 mM EDTA, 200 mM NaCl, 0.2% sodium dodecyl sulfate) including 0.1 mg of proteinase K/ml. One microliter of the lysate diluted 1:10 in H_2O was analyzed by multiplex PCR (0.5 U of Platinum *Taq* DNA polymerase [Invitrogen], 1.5 mM $MgCl_2$, 0.2 mM [each] deoxynucleoside triphosphate, 1× Rediload [Research Genetics], 1× PCR buffer [Invitrogen; 10 mM Tris-Cl {pH 8.3}, 50 mM KCl, 0.02 mg of bovine serum albumin/ml], five primers at 0.2 μM each). Primers are *Nfib* specific (*a* and *b*), *lacZ* specific (*c*), or mouse Y chromosome specific (*SRY-1* and *-2*); sequences are as follows: *a*, 5′-GCTGAGTTGGGAGATTGTGTC-3′; *b*, 5′-TTCTGCTTGATTTCGGGCTTC-3′; *c*, 5′-CATCGTAACCGTGCATCT GCC-3′; *SRY-1*, 5′-AACAACTGGGCTTTGCACATTG-3′; *SRY-2*, 5′-GTTTA TCAGGGTTTCTCTCTAGC-3′). PCR products were resolved on 2.0% agarose gels and visualized with ethidium bromide.

PCR and QPCR transcript analysis. Total RNA was isolated with TRIzol reagent (Invitrogen), and cDNA was generated from 2 to 5 μg of RNA with Superscript II reverse transcriptase (Invitrogen) and random primers as recommended by the manufacturer. *Nfib* transcripts were analyzed by PCR with an exon 1-based sense primer (5′-GATCGGCCTCACGGGCCGATGATGTATT CTCCCATCTG-3′) and an exon 4-based antisense primer (5′-CTCTGATACA TTGAAGACTCCG-3′), and products were resolved on a 2.5% agarose gel. Transcript levels of all genes shown were quantified by quantitative PCR (QPCR) with a Bio-Rad iCycler real-time PCR machine and gene-specific primers that span multiple exons as described previously (61). Primer sequences for the genes quantified are available upon request.

Tissue preparation and lacZ detection. Embryos were harvested at various times after detection of a coital plug. For total lung DNA analysis, either the dissected left lobe (embryonic day 18.5 [E18.5]) or the whole lung (E15.5) was harvested into 1 ml of 2 M NaCl–2 mM EDTA in phosphate-buffered saline (PBS) and sonicated on ice, and DNA content was assayed fluorimetrically as described previously (32) with a 96-well plate fluorimeter and purified calf thymus DNA as a standard. Whole thoraces were immersed in cold 4% paraformaldehyde (PFA) overnight, washed in PBS, dehydrated in ethanol, embedded in paraffin, and transversely sectioned at 5 μm for hematoxylin and eosin (H&E) staining and immunohistochemistry.

β-Gal staining was performed on cryostat sections of frozen fixed tissues. Lungs were fixed in PBS containing 0.2% glutaraldehyde, 5 mM EGTA (pH 7.3), and 0.1 M $MgCl_2$ for 3 h on ice and rinsed three times for 15 min with cold PBS. Fixed tissues were cryoprotected overnight in cold 30% sucrose in 1× PBS and then embedded in OCT embedding medium and snap-frozen on dry ice. Cryostat sections of frozen tissue (10 μm) were loaded onto polylysine-coated slides and allowed to dry at room temperature for 2 h and incubated in β-Gal solution (5 mM potassium ferricyanide, 5 mM potassium ferrocyanide, 1 mg of X-Gal [5-bromo-4-chloro-3-indolyl-β-D-galactopyranoside]) in buffer (100 mM sodium phosphate [pH 7.3], 2 mM $MgCl_2$, 0.01% sodium deoxycholate, 0.02% NP-40) at room temperature for 6 h. Stained sections were washed three times in PBS and then postfixed in distilled water containing 2% glutaraldehyde, 2% PFA, and 0.1 M sodium cacodylate for 1 h at 4°C. The slides were rinsed in three changes of cold PBS for 10 min each, cleared in distilled water for 5 min, and then counterstained with 0.1% nuclear fast red in 5% aluminum sulfate for 2 min, washed in running water, dehydrated, and topped with coverslips for analysis.

For whole-mount staining fixed lungs were washed and immediately incubated in β-Gal solution at room temperature overnight without cryoprotection. Stained lung lobes were washed three times with PBS and postfixed as described above, and washed left lobes were photographed through a dissecting microscope.

Brain sectioning and staining. Brains were perfused with 4% PFA, fixed overnight in 4% PFA, and stored in PBS until use. Brains were blocked in 3% agar and cut at 40 to 50 μm on a vibratome (Leica, Deerfield, Ill.). The sections were counterstained with 2% Mayer's hematoxylin (Sigma Chemical Co.) for 6 min, or alternatively with 1% thionin, rinsed, dehydrated, and mounted for analysis.

Immunohistochemistry. All procedures were performed at room temperature. Brain sections were washed three times in PBS and blocked in a solution of 2% (vol/vol) serum and 0.2% (vol/vol) Triton X-100 (Sigma) in PBS for 2 h. Normal goat serum (S-1000; Vector Laboratories, Burlingame, Calif.) or normal donkey serum (017-000-121; Jackson ImmunoResearch Laboratories, West Grove, Pa.) was used as the blocking agent. The sections were incubated with the primary antibody, rabbit anti-glial fibrillary acidic protein (GFAP; 1:30,000; Z0334; Dako, Glostrup, Denmark) or rat anti-L1 (1:5,000; MAB5272; Chemicon, Temecula, Calif.), overnight. Sections were then washed three times in PBS and incubated with the biotinylated secondary antibody (biotinylated goat anti-rabbit secondary antibody [1:500; Vector Laboratories] or biotinylated donkey anti-rat secondary antibody [1:500; Jackson ImmunoResearch Laboratories]) for 2 h. After three washes in PBS, sections were incubated in avidin-biotin solution (1:500; Vector Laboratories) for 1 h, followed by three washes in PBS. Sections were then immersed in a nickel–3,3′-diaminobenzidine (DAB; D-5905; Sigma)–chromogen solution (2.5% nickel sulfate and 0.02% DAB in 0.175 M sodium acetate) activated with 0.01% (vol/vol) H_2O_2 until a dark purple-black precipitate formed. Sections were washed in PBS, mounted, and placed on coverslips in DPX mounting medium (Electron Microscopy Services). Labeling was analyzed with an upright light microscope (Leica). Images were made with a PowerPhase digital camera (PhaseOne, Copenhagen, Denmark) directly into Adobe Photoshop software.

Immunohistochemistry for α smooth muscle actin (αSMA) was performed essentially as described previously (41). The smooth muscle differentiation marker αSMA was detected with mouse monoclonal anti-αSMA 1A4 (1:20,000; Sigma). Staining was performed with the Mouse on Mouse kit (Vector Laboratories). Biotinylated secondary antibodies were used with a nickel-enhanced DAB protocol essentially as described for the brain except that slides were counterstained with nuclear fast red.

RESULTS

***Nfib* gene targeting and confirmation of *Nfib* null allele.** We constructed a replacement-type targeting vector by replacing the most 3′ 523 bp of exon 2 and the first 177 bp of intron 2 with a translational-fusion β-Gal reporter gene and a neomycin resistance gene (*lacZ* and *Neo*, respectively, in Fig. 1A). Since exon 2 encodes both the DNA-binding and dimerization activities of NFI, homologous recombination of the native gene and the targeting vector should generate a null allele. SacI digests of targeted ES cell genomic DNA analyzed with a DNA probe that maps external to the targeted region generated 8.2-kb targeted-allele and 22.7-kb native-allele fragments (Fig. 1A) in heterozygous targeted ES cells. A Southern blot screen of 80 G418-resistant ES clones identified 6 clones harboring a single targeted mutation, and a composite of the results of the screen is shown (Fig. 1B). Further Southern blot analyses using *Neo*- and *lacZ*-specific probes showed that *Nfib*-targeted clones harbored no other vector integrations. PCR analyses confirmed homologous recombination of the 3′ flanking region (data not shown).

We injected two ES clones heterozygous for the targeted *Nfib* mutation (*Nfib*$^{-/+}$) into C57BL/6 mouse blastocysts to generate chimeras. Male chimeras of one ES clone were crossed to Black Swiss, 129S6, FVB/N, and C57BL/6 strains, and genomic DNA from tail biopsy samples of the progeny was screened by PCR for the mutated allele. Both ES clones transmitted the mutant allele into the germ line, and the phenotypes of mice derived from the two ES clones were indistinguishable. To confirm that the targeted *Nfib* allele was null, we analyzed
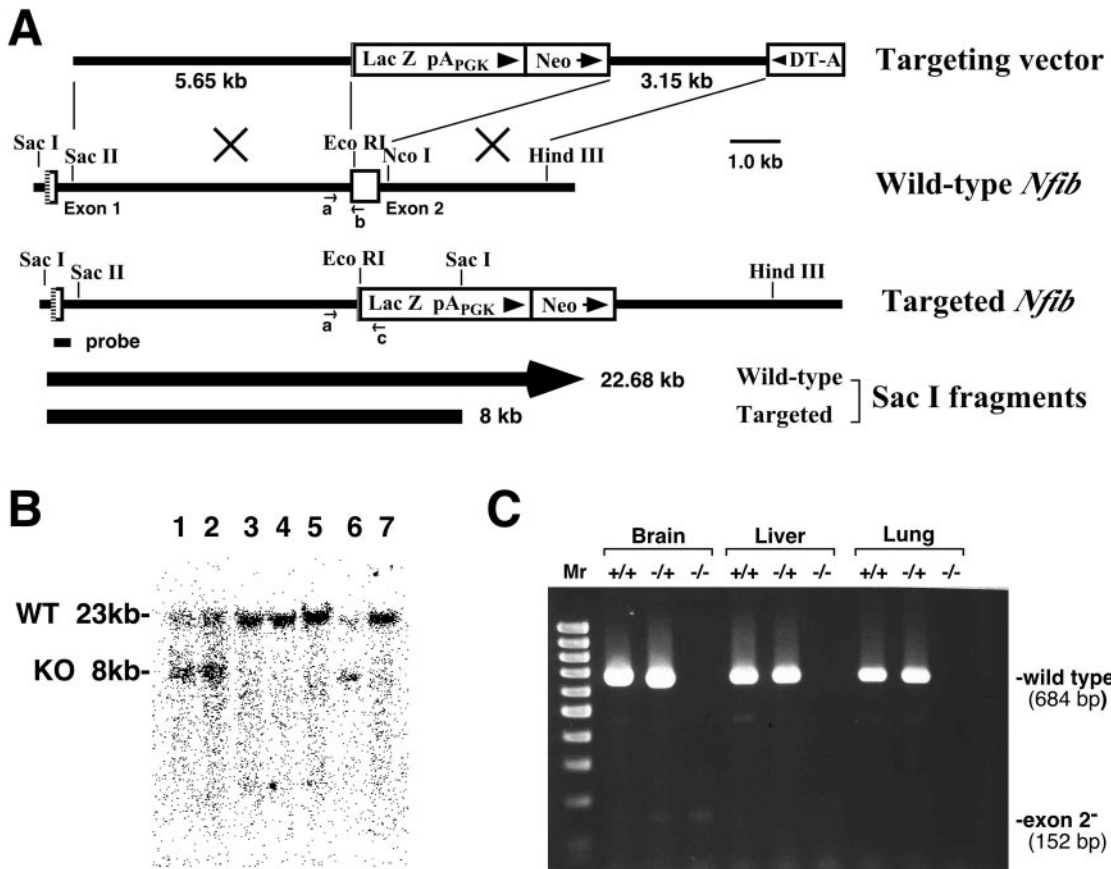
FIG. 1. Disruption of *Nfib* gene and generation of null allele. (A) *Nfib* targeting vector (top) generated by replacement of most of exon 2 with the coding sequence for an NLS–β-Gal translational fusion protein and a PGK-neo selection cassette. Correct targeting of the *Nfib* locus causes loss of a 22.68-kb SacI fragment and gain of an 8-kb SacI fragment (arrows) on screening with the indicated probe. (B) Detection of targeted ES clones by Southern blotting. Genomic DNA was digested with SacI, analyzed on a 0.8% agarose gel, transferred to a nylon membrane, and hybridized with the ^{32}P-labeled probe fragment indicated in panel A. The WT allele yields an ~23-kb band, while the targeted allele shows an ~8-kb band. Lanes 1, 2, and 6 contain both WT and targeted alleles. (C) Loss of full-length *Nfib* transcripts from brains, livers, and lungs of *Nfib*$^{-/-}$ mice. RNA from the indicated tissues of WT, *Nfib*$^{-/+}$, and *Nfib*$^{-/-}$ mice was isolated and reverse transcribed, and the cDNA was analyzed by PCR with the exon 1 and exon 4 primers described in Materials and Methods. PCR products were analyzed on 2.0% agarose gels, and three products were detected, a major 684-bp band containing exons 1 to 4 seen in cDNA from WT and *Nfib*$^{-/+}$ mice and a much weaker ~152-bp band lacking exon 2 seen in cDNA from *Nfib*$^{-/+}$ and *Nfib*$^{-/-}$ mice. Another low-abundance product, migrating at approximately 450 bp, was generated from WT and *Nfib*$^{-/+}$ cDNA but not from *Nfib*$^{-/-}$ cDNA. This product may represent aberrantly spliced *Nfib* transcripts. Lane Mr, molecular weight markers.

brain, liver, and lung *Nfib* transcripts isolated from E17.5 littermates of each *Nfib* genotype. Total RNA was reverse transcribed, and the cDNA then used as the template in PCRs with *Nfib* exon 1-specific (forward) and exon 4-specific (reverse) primers (Fig. 1C). The major product generated from wild-type (WT; *Nfib*$^{+/+}$) and heterozygote (*Nfib*$^{-/+}$) brain, liver, and lung cDNA corresponds to a predicted 684-bp product that includes exon 2 (532 bp), exon 3 (54 bp), and parts of exons 1 and 4 (Fig. 1C, lanes +/+ and −/+). However, no such product was generated from *Nfib* homozygous mutant (*Nfib*$^{-/-}$) brain, liver, and lung cDNA (Fig. 1C, lanes −/−). A much less abundant product having a migration corresponding to that of a predicted 152-bp amplicon was generated only from *Nfib*$^{-/+}$ and *Nfib*$^{-/-}$ brain cDNA. This product likely represents an *Nfib* transcript containing exon 1 spliced directly to exon 3, therefore lacking exon 2. Because exon 1 ends at codon base 3 and exon 3 begins at codon base 2, such an

aberrantly spliced *Nfib* transcript would encode a 35-amino-acid missense polypeptide that terminates at a TAG codon in exon 4. These data indicate that replacement of all but 3 residues encoded by exon 2 with the β-Gal fusion protein generates a null allele of *Nfib*.

Lung maturation defects in *Nfib*-deficient mice. A previous study showed that mice with an insertion of a *lacZ* translational fusion gene into the same EcoRI site in exon 2 of *Nfib* targeted here exhibited defects in lung maturation (22). We therefore examined lung development in our *Nfib*-null mice. Mouse lung maturation occurs relatively late in gestation, with final prenatal maturation (sacculation) occurring from E16.5 to P3 (10). Histological examination of lungs in E17.5 *Nfib*-deficient mice showed that lungs from *Nfib*$^{-/-}$ mice were severely defective in maturation, while those from *Nfib*$^{-/+}$ animals had a clear developmental delay in maturation. WT lungs at E17.5 were well sacculated (Fig. 2A), while lungs from *Nfib*$^{-/+}$ mice had
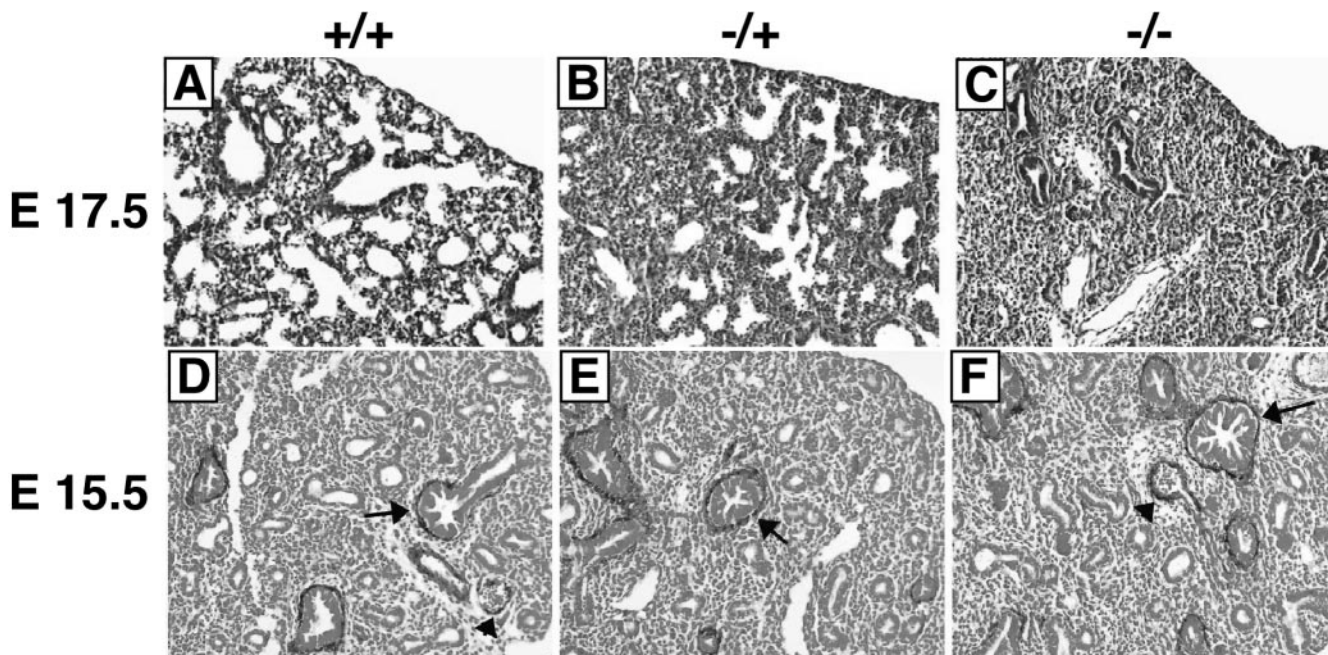
FIG. 2. Decreased lung maturation in $Nfib^{-/+}$ and $Nfib^{-/-}$ mice. Transverse sections of E17.5 lungs (A to C) were stained with H&E, and E15.5 lungs (D to F) were stained with a monoclonal antibody against a smooth muscle actin (αSMA) and counterstained with nuclear fast red. E17.5 $Nfib^{+/+}$ lungs (A) show normal sacculation (open areas that produce a "Swiss cheese" appearance), while $Nfib^{-/+}$ lungs (B) have reduced sacculation and $Nfib^{-/-}$ lungs (C) show essentially no sacculation. E15.5 lungs of all three genotypes ($Nfib^{+/+}$ [D], $Nfib^{-/+}$ [E], and $Nfib^{-/-}$ [F]) showed similar cellular morphologies and αSMA staining in smooth muscle surrounding bronchioles (arrows) and vessels (arrowheads). Mice were in the Black Swiss (A to C) and FVB/N (D to F) backgrounds.

smaller saccules (Fig. 2B) and lungs of $Nfib^{-/-}$ mice completely lacked saccules (Fig. 2C). The morphology of the E17.5 $Nfib^{-/-}$ lungs resembled that of less-mature WT E15.5 lungs (Fig. 2, compare panels C and D). To assess the approximate time in development at which maturation was arrested, we examined the morphology of E15.5 WT, $Nfib^{-/+}$, and $Nfib^{-/-}$ lungs (Fig. 2D to F, respectively). Unlike the case at E17.5, at E15.5 the WT and mutant lungs had similar morphologies with dense mesenchyme and no saccules. In addition, levels of smooth muscle actin expression around the bronchioles (Fig. 2D to F) and vessels (Fig. 2D and F) in WT and mutant mice were similar. These data indicate that lung development in $Nfib^{-/-}$ mice appears arrested between E15.5 and E16.5 at the late-pseudoglandular-to-early-canalicular stage of development and that $Nfib^{-/+}$ mice have a less severe phenotype of delayed lung maturation.

Perinatal lethality in *Nfib*-deficient mice. The difference in severity of the lung maturation defects between $Nfib^{-/-}$ and $Nfib^{-/+}$ animals was confirmed by the finding that no $Nfib^{-/-}$ animals survived for 24 h after birth (Table 1; 10 litters, 0 of 23 $Nfib^{-/-}$ animals alive at day 1), while ~60% of the predicted number of $Nfib^{-/+}$ animals survived (34 of 58 predicted $Nfib^{-/+}$ animals). The lethality appears to be perinatal since the genotypes of E17.5 to E18.5 embryos were present at nearly the expected Mendelian frequency of 1:2:1 (66 $Nfib^{+/+}$ mice, 115 $Nfib^{-/+}$ mice, and 70 $Nfib^{-/-}$ mice; 31 litters). Compared to $Nfib^{+/+}$ animals in the same litters, only ~55% of $Nfib^{-/+}$ animals in the C57BL/6 strain survived to genotyping, suggesting that the delay in lung maturation in $Nfib^{-/+}$ animals reduces early postnatal survival in this strain (Table 2; 70

$Nfib^{-/+}$ mice survived to day 14 versus 124 $Nfib^{+/+}$ mice; 26 litters). Surprisingly, little or no loss of heterozygotes was seen during backcrossing to the FVB/N strain, indicating that this reduction in heterozygote survival is strain specific (Table 2; 83 $Nfib^{-/+}$ mice versus 75 $Nfib^{+/+}$ mice survived to day 14; 17 litters). Histological evaluation of heterozygote E18.5 lungs showed that delays in sacculation were indistinguishable among the strains. Whether this difference in survival of *Nfib*-deficient heterozygotes among strains is dependent on modifier genes and/or maternal rearing differences remains to be determined. These data strongly support a model for haploin-sufficiency at the *Nfib* locus.

Changes in gross morphology, DNA content, and epithelial differentiation markers in lungs of *Nfib*$^{-/-}$ mice. A previous report on the insertion of a lacZ transgene into exon 2 of *Nfib*

TABLE 1. Lethality in *Nfib*-deficient animals[a]

Status of animal on day 1	No. of animals of genotype:		
	$-/-$	$-/+$	$+/+$
Live	0	34	29
Dead	23	2	0
Expected	29	58	29

[a] Heterozygous $Nfib^{-/+}$ mixed Black Swiss/129S6 strain animals were bred, and the numbers of animals of different genotypes that were born and survived to day 1 after birth are shown. The expected numbers for heterozygote $Nfib^{-/+}$ and homozygote $Nfib^{-/-}$ animals are twice and equal to, respectively, the number of $Nfib^{+/+}$ animals obtained. No $Nfib^{-/-}$ animals survived to day 1 after birth from 10 litters. The apparent reduction in $Nfib^{-/+}$ animals may be due to cannibalism of some dead pups by the mothers.

TABLE 2. Loss of $Nfib^{-/+}$ animals during backcrossing of heterozygous $Nfib^{-/+}$ animals to the C57BL/6 but not the FVB/N strain[a]

Strain	No. of live animals of genotype:			
	$-/+$		$+/+$	
	Observed	Expected	Observed	Expected
C57BL/6	70	124	124	124
FVB/N	83	75	75	75

[a] Heterozygous $Nfib^{-/+}$ males were bred with WT C57BL/6 and FVB/N females, and the numbers of $Nfib^{-/+}$ and $Nfib^{+/+}$ animals alive at day 14 after birth were recorded. Twenty-six and 17 litters were examined during 5 backcross generations into C57BL/6 and FVB/N, respectively. The expected numbers are derived from the number of $Nfib^{+/+}$ progeny obtained.

TABLE 3. Total body weights and DNA contents of the left lung[a]

Genotype	No. of pups	Total body wt (g)	Left lung DNA/total body wt (μg/g)
$Nfib^{+/+}$	6	1.18 ± 0.065	38.6 ± 3.93
$Nfib^{-/+}$	12	1.21 ± 0.124	51.9 ± 5.08
$Nfib^{-/-}$	5	1.38 ± 0.083	73.1 ± 10.47

[a] Data are means ± standard deviations.

described the lungs of the resulting mice as hypoplastic (22). We dissected lungs from our E15.5 and E18.5 WT and *Nfib*-deficient embryos to assess their gross morphology. The gross morphologies of WT and *Nfib*-deficient lungs were almost indistinguishable at E15.5 (Fig. 3A; left lobes are shown for comparison). Upon close inspection, slight indentations were detected on the surfaces of $Nfib^{-/-}$ lungs (Fig. 3A). At later times in gestation these indentations became more pronounced and obvious surface clefts or crevices were seen in all $Nfib^{-/-}$ lungs examined (Fig. 3B and C). Despite the presence of these defects in the pleural surface, $Nfib^{-/-}$ lungs were not obviously hypoplastic.

To determine whether there was overall cell loss (hypoplasia) in the $Nfib^{-/-}$ lungs, we assessed the left lung DNA contents and total body weights of E18.5 embryos (Table 3). While the total body weights of WT, $Nfib^{-/+}$, and $Nfib^{-/-}$ animals

were similar, there was a substantial increase in the total DNA in the lungs of $Nfib^{-/-}$ animals, resulting in an increased ratio of DNA content to total body weight for these animals (Table 3; $Nfib^{-/-}$ versus $Nfib^{+/+}$). Thus while differentiation of type I and II epithelial cells appears defective in the $Nfib^{-/-}$ lungs (see below), there is an apparent increase in cell number in the $Nfib^{-/-}$ lungs. These data indicate that, rather than hypoplasia or cell loss in the $Nfib^{-/-}$ lungs, there is instead an increase in DNA content, suggesting a defect in either the turning off of cell proliferation or in apoptosis during lung maturation (62).

We also measured proliferating cell nuclear antigen (PCNA) levels in WT and *Nfib* mutant lungs to assess overall levels of cell proliferation. PCNA transcripts were increased approximately fourfold at E18.5 in $Nfib^{-/-}$ versus $Nfib^{+/+}$ lungs, suggesting that higher levels of proliferation occurred in the mutant lungs (Table 4). This apparent increase in proliferation is consistent with the thickened mesenchyme and increased DNA content in $Nfib^{-/-}$ lungs and may reflect a failure of the normal reduction in mesenchymal proliferation seen during lung maturation (62). As an initial screen for signaling molecules that may influence cell proliferation during lung maturation, we used QPCR to assess the levels of *Fgf-10*, *Fgf-7*, and *Midkine* transcripts in WT and $Nfib^{-/-}$ lungs. Fibroblast growth factor signaling is essential for early lung development, and loss of *Fgf-10* results in a lack of branching morphogenesis (53). While there was an ~2-fold increase in *Fgf-10* levels and no change in *Fgf-7* levels in E18.5 $Nfib^{-/-}$ lungs relative to $Nfib^{+/+}$ lungs, there was an ~11-fold increase in *Midkine* expression in the mutant lungs (Table 4). Since increased *Midkine* levels have been associated with the decreased lung maturation seen in glucocorticoid receptor-deficient mice (28) and with lung vascular remodeling after hypoxia (48), it will be important to
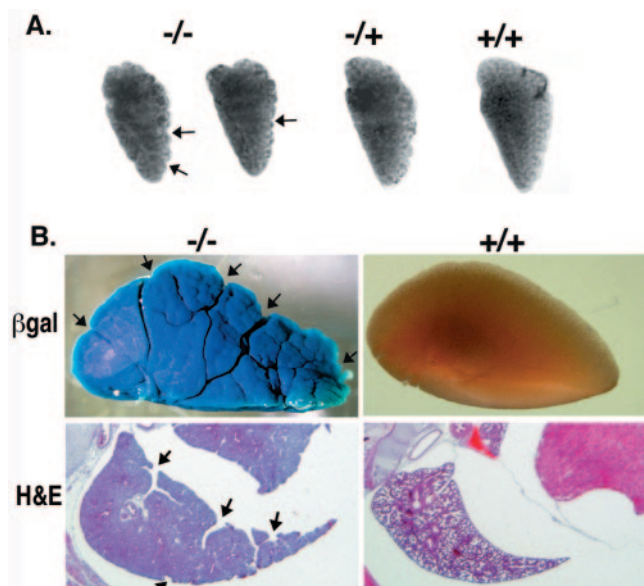

FIG. 3. Gross morphological changes in $Nfib^{-/-}$ lungs. Dissected left lobes are shown unstained at E15.5 (A), whole mount stained for β-Gal at E18.5 (B; βgal), and H&E stained in transverse section at E18.5 (B; H&E). Although there is no gross change in overall size and shape, minor surface indentations seen in E15.5 lungs appear more striking as deep clefts or ruffles at E18.5. *lacZ* expression is detected in $Nfib^{-/-}$ lungs but not $Nfib^{+/+}$ lungs (B). Arrows, surface indentations and clefts.

TABLE 4. Transcript levels in $Nfib^{-/+}$ and $Nfib^{-/-}$ lungs relative to those in $Nfib^{+/+}$ lungs[a]

Gene	Relative level in E18.5 lungs of:	
	$Nfib^{-/+}$ mice	$Nfib^{-/-}$ mice
PCNA	1.3 ± 0.1	3.8 ± 0.5
Fgf-10	1.0 ± 0.1	2.2 ± 0.8
Fgf-7	1.1 ± 0.4	0.7 ± 0.2
Midkine	2.1 ± 0.6	11.0 ± 2.1
SP-A	0.8 ± 0.2	0.4 ± 0.1
SP-B	0.5 ± 0.2	0.2 ± 0.1
SP-C	0.7 ± 0.2	0.5 ± 0.1
SP-D	0.5 ± 0.1	0.1 ± 0.04
Aqp-1	0.6 ± 0.1	0.3 ± 0.1
ENaC	0.6 ± 0.1	0.3 ± 0.1

[a] Transcript levels, measured by QPCR and normalized to β2-microglobulin levels in each sample, were divided by those found in $Nfib^{+/+}$ littermates and expressed as means ± standard deviations. At least two independent litters were used for analysis of each gene, with multiple animals of each genotype.

assess *Midkine*'s role in the apparent increase in mesenchymal cell density in *Nfib*^{−/−} lungs.

To determine if morphological immaturity corresponded with reduced expression of maturation-associated genes, we examined the transcript levels at E18.5 of a number of genes whose expression is known to increase from E16.5 to E18.5 in normal mouse lung development. Lung maturation from E16.5 to E18.5 is characterized by large increases in markers of type II epithelial and type I squamous epithelial cell differentiation (65). Using QPCR we showed that a number of type II cell markers, including surfactant protein A (SP-A), SP-B, SP-C, and SP-D, are greatly reduced in *Nfib*^{−/−} lungs and partially reduced in *Nfib*^{−/+} lungs relative to WT lungs at E18.5 (Table 4). Also, type I cell markers *Aquaporin-1* (*Aqp-1*) and the epithelial sodium channel gene (*ENaC*) were strongly reduced in *Nfib*^{−/−} lungs and partially reduced in *Nfib*^{−/+} lungs (Table 4). These data indicate that loss of *Nfib* results in a significant reduction in expression of terminal differentiation markers of type II and type I cells, suggesting that *Nfib* is essential for the normal differentiation of these cells.

Nfib::lacZ expression during lung development. Lung development requires many reciprocal epithelial-mesenchymal inductions (see references 25 and 54 for reviews). While our previous in situ data showed that *Nfib* is highly expressed in the developing lung (6), the cellular expression pattern was not determined. To identify the specific cell compartments where *Nfib* is expressed during lung development, we stained lungs of mice heterozygous for the *Nfib*::*lacZ* allele for β-Gal activity. *Nfib*::*lacZ* was uniformly expressed at high levels throughout the mesenchyme at E14.5, whereas weaker expression was detected in a few scattered epithelial cells at this time (Fig. 4A). *Nfib*::*lacZ* was expressed at similar levels in most epithelial and mesenchymal cells at E16.5, with increased expression in smooth muscle (Fig. 4B). At E18.5, *Nfib*::*lacZ* was expressed in a subset of both proximal and distal epithelial cells, while mesenchymal expression was decreased but still present in the smooth muscle (Fig. 4C and D). LacZ staining was not detected in WT E18.5 lung (Fig. 4E). In adult lung *Nfib*::*lacZ* was expressed primarily in the bronchiolar epithelium and type II cells (Fig. 4F). Preliminary immunohistochemistry with *Nfib*-specific antibodies supports this pattern for endogenous *Nfib* in WT mice (C. Bachurski, unpublished data). These data indicate that *Nfib* could play essential roles in either the lung mesenchyme or epithelium during late prenatal lung maturation.

Nfib^{−/−} mice display agenesis of the corpus callosum, enlargement of the lateral ventricles, and malformation of midline glial populations. We showed previously that loss of *Nfia* resulted in major neurological defects, including agenesis of the corpus callosum and defects in other forebrain commissures (11, 56). Although the previous study of a *lacZ* insertion into the *Nfib* locus reported no effects on brain development (22), we found multiple profound defects in brain development in our *Nfib*^{−/−} mice. As seen previously in our *Nfia*^{−/−} mice (56), *Nfib*^{−/−} mice exhibit agenesis of the corpus callosum on both mixed Black Swiss/129S6 (Fig. 5A to C) (*n* = 4) and C57BL/6 (Fig. 5D to I) (*n* = 3) backgrounds. This was evident with hematoxylin staining (Fig. 5A to F) and was confirmed by L1 cell adhesion molecule (CAM) immunohistochemistry, which labels axonal tracts (Fig. 5G to I). On the mixed Black

Swiss background, most heterozygous *Nfib*^{−/+} animals also displayed a callosal phenotype (*n* = 8 of 11), with the formation of Probst bundles at the midline (*n* = 11 of 11; Fig. 5B). However this phenotype in heterozygotes was less penetrant (*n* = 1 of 7) after backcrossing the allele onto a C57BL/6 background (Fig. 5E).

Surviving postnatal *Nfia*^{−/−} mice on a mixed Black Swiss-129S6-C57BL/6 background exhibit severe hydrocephalus (11). Although *Nfib*^{−/−} mice die at birth, precluding analysis of postnatal hydrocephalus, embryonic *Nfib*^{−/−} mice have larger ventricles (Fig. 5C and F) than their WT and heterozygote littermates on both mixed Black Swiss and C57BL/6 backgrounds. These data suggest that both *Nfib* and *Nfia* may influence cerebrospinal fluid transport and/or production in the brain.

Midline glial populations are important for the formation of the corpus callosum, as they secrete guidance factors, such as Slit2, that guide callosal axons both before and after they cross the midline (58, 59). Figure 6 shows an immunohistochemical analysis of GFAP expression. Three midline glial populations are evident in WT animals: the glial wedge (GW), glia within the indusium griseum (IGG), and the midline zipper glia (MZG; Fig. 6D) (57). *Nfib*^{−/−} mice showed a reduction in GFAP expression at the midline, which likely reflects a loss or reduction in these glial populations. This phenotype is similar to that observed in *Nfia*^{−/−} mice (56). *Nfib*^{−/−} mice display a complete absence of GFAP labeling in the regions of both the IGG and the MZG (Fig. 6F and L). Furthermore, although a few glial cells were present, the GW was greatly reduced in the *Nfib*^{−/−} animals (Fig. 6F and L). Since there are NFI binding sites in the GFAP gene promoter, these results, together with our results for *Nfia*^{−/−} mice (56), suggest that NFI genes may regulate both GFAP expression and glial development. Further evidence for such regulation is that *Nfib*^{−/+} mice on a C57BL/6 background display lower levels of expression of GFAP than their *Nfib*^{+/+} littermates (compare Fig. 6K and J). Although all three midline glial populations were present in *Nfib*^{−/+}animals on both the Black Swiss and C57BL/6 background, the IGG appeared disorganized on the Black Swiss background, probably due to the formation of Probst bundles at the midline (Fig. 6E).

We showed previously that GFAP expression is decreased in *Nfia*^{−/−} brains relative to WT brains (11). Since we observed a decrease in GFAP-positive midline glial cells in *Nfib*^{−/−} brains, we examined GFAP transcript levels in *Nfib*^{−/−} whole brains. Although GFAP transcript levels were reduced ∼5-fold in *Nfib*^{−/−} brains relative to WT, this decrease is less than the ∼10-fold decrease seen in *Nfia*^{−/−} brains (Table 5). While examining the expression of genes proposed to influence forebrain development in *Nfia* KO mice, we noted that *Tbr2* transcript levels were increased 1.9-fold in *Nfia*^{−/−} brains relative to *Nfia*^{+/+} brains (Table 5). However, *Nfib*^{−/−} brains had no higher levels of *Tbr2* transcripts than did *Nfib*^{+/+} brains (Table 5). Thus, while the neuroanatomical defects in the *Nfib*^{−/−} brains appear more severe than those of *Nfia*^{−/−} brains, the changes in *GFAP* and *Tbr2* expression in *Nfib*^{−/−} brains are less than those observed in *Nfia*^{−/−} animals. In addition, there were no apparent changes in the levels of transcripts for some other genes that have been proposed to play a role in callosum formation and forebrain development, including *Slit2*, *Robo1*
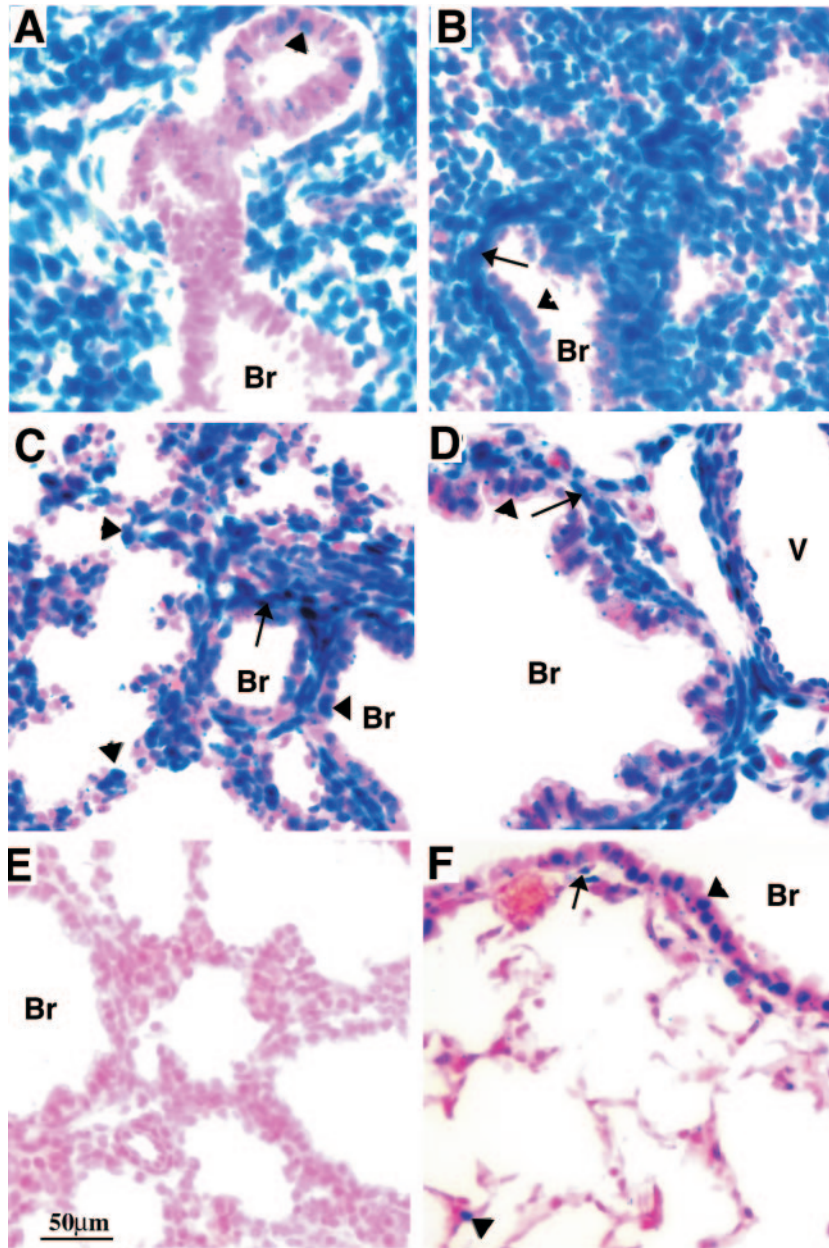
FIG. 4. Expression of β-Gal from the *Nfib-lacZ* allele in *Nfib*$^{-/+}$ lungs. Frozen sections of lungs of E14.5 (A), E16.5 (B), E18.5 (C and D), and adult *Nfib*$^{-/+}$ (F) or E18.5 *Nfib*$^{+/+}$ (E) mice were stained for β-Gal activity. β-Gal expression was predominantly mesenchymal at E14.5. Smooth muscle was strongly positive from E16.5 to E18.5, with reduced staining in adult lung (arrows). Expression decreased in the mesenchyme and increased in both proximal and distal epithelial cells from E16.5 through E18.5. β-Gal expression was mainly in a subset of the bronchiolar epithelium and type II cells in adult lung. Br, bronchiole; V, vessel; arrows, smooth muscle; arrowheads, epithelium. The scale bar (E) applies to all panels. Mice were in the FVB/N background.

to -*3*, *DCC*, *Netrin*, and others (Table 5). Thus the reduction in *GFAP* transcripts is the only consistent change in gene expression so far detected in *Nfib*$^{-/-}$ brains and is likely due at least in part to the observed loss of GFAP expression from specific midline glial cells.

Nfib regulates development of the hippocampus and the basilar pons. *Nfib*$^{-/-}$ mice also displayed severe disruptions in the formation of the hippocampus (Fig. 7). At E17.5 the dentate gyrus was absent (Fig. 7A, C, and F) and the entire CA3

region (Fig. 7A) appeared to be absent or severely reduced (Fig. 7C and F). The fimbria, which contains the efferent projections from the hippocampus, was also greatly reduced (compare Fig. 7C with A and B and F with D and E). This phenotype was evident on both the Black Swiss background and the C57BL/6 background, but the losses appeared to be more severe on the C57BL/6 background. To ask whether the defects were due to degeneration of these areas or, conversely, to a delay in development, we examined the hippocampal primor-
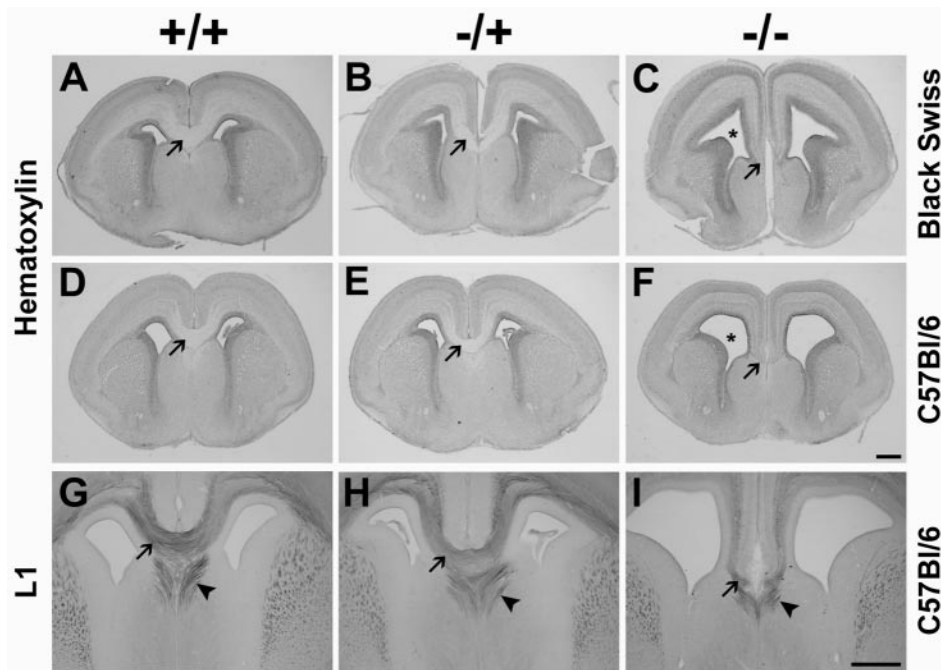
FIG. 5. Agenesis of the corpus callosum in *Nfib*$^{-/-}$ mice. Coronal 50-μm vibratome sections from E17.5 *Nfib* brains on either a Black Swiss (A to C) or C57BL/6 (D to F) background were mounted and stained with hematoxylin (A to F) or stained free-floating with an antibody against L1 CAM (G to I). Arrows in each panel indicate the presence or absence of the corpus callosum; arrowheads (G to I) indicate the presence of the fornix. Probst bundles were evident in *Nfib*$^{-/+}$ mice on a mixed Black Swiss background (B). *Nfib*$^{-/-}$ mice displayed enlarged ventricles (C and F; asterisks). Scale bars: 2 mm (F; applies to panels A to F) and 1 mm (I; applies to panels G to I).

dium at E15.5 (Fig. 7G to I). Even at E15.5 defects in hippocampal development were present. The entire hippocampal primordium, including the fimbria, was reduced in size. These data suggest that *Nfib* may regulate hippocampal cell proliferation and, since the CA1 region was less affected, possibly the regionalization of the hippocampus into different subfields.

Previous studies showed that *Nfib*, *Nfia*, and *Nfix* are highly expressed in the basilar pons (6, 16), a hindbrain nucleus that provides significant mossy fiber input to the cerebellum. To investigate the role of *Nfib* in the development of the basilar pons, we examined *Nfib*$^{-/-}$ hindbrains at E16.5 to E18.5 on C57BL/6 and Black Swiss backgrounds. The basilar pons is well formed at E18.5 in WT (*n* = 3) and heterozygote (*n* = 5) animals (Fig. 8A and B). However, the basilar pons was virtually absent in *Nfib*$^{-/-}$ brains (*n* = 4), with only a small cap of cells remaining (Fig. 8C). The pontine phenotype was evident from E16.5 to E18.5 in both Black Swiss (*Nfib*$^{+/+}$, *n* = 3; *Nfib*$^{-/+}$, *n* = 5; *Nfib*$^{-/-}$, *n* = 4) and C57BL/6 backgrounds. The rest of the hindbrain, including another precerebellar nucleus, the inferior olive, appears normal (Fig. 8B and C). In addition, the cerebellum is present and the normal lamination can be identified in the mutant. However, although foliation begins at this age in WT and heterozygous mice, the cerebellum appears unfoliated in *Nfib*$^{-/-}$ mice (Fig. 8C versus A). It will be of interest to determine whether this apparent decreased foliation reflects changes in cerebellar cell proliferation or differentiation.

Expression of the other three *Nfi* genes in *Nfib*-deficient animals. To determine if loss of *Nfib* affected the expression levels of the other three *Nfi* genes, we assessed *Nfi* transcript levels in the lungs and brains of E18.5 WT and *Nfib*$^{-/-}$ animals. There were ~5.1, 3.3, and 2.8-fold increases in *Nfia*, *Nfic*, and *Nfix* expression, respectively, in *Nfib*$^{-/-}$ lungs relative to WT lungs (Table 6). Thus, of the three NFI genes remaining in *Nfib*$^{-/-}$ mice, the *Nfia* gene has the largest increase in expression in lung. In E18.5 whole brain, there was a 2.2-fold increase in *Nfia* expression but no significant change in *Nfic* or *Nfix* expression (Table 6). These data indicate that there were greater changes in the expression of the remaining *Nfi* genes in the lungs of *Nfib*-deficient animals than in the brains of these animals and that *Nfia* exhibited the greatest changes in both tissues. The significance of these changes and their relationship to the phenotypes seen in the tissues are being examined.

DISCUSSION

By replacing exon 2 of *Nfib* with a *lacZ* translational fusion construct (Fig. 1) we have shown that *Nfib* is essential for perinatal survival (Tables 1 and 2), late fetal lung maturation (Fig. 2 and 3; Tables 3 and 4), and brain development (Fig. 5 to 8 and Table 5). Loss of *Nfib* results in apparent arrest of fetal lung maturation at the late-pseudoglandular or early-canalicular stage, as indicated by both morphology (Fig. 2) and reduced expression of several late lung differentiation markers (Table 4). In addition, severe defects in development of the corpus callosum (Fig. 5), specific midline glial populations (Fig. 6), the hippocampus (Fig. 7), and the pons (Fig. 8) show that *Nfib* is essential for the proper development of both forebrain and hindbrain structures. Since our previous studies indicated that loss of *Nfia* resulted in callosal agenesis and loss of
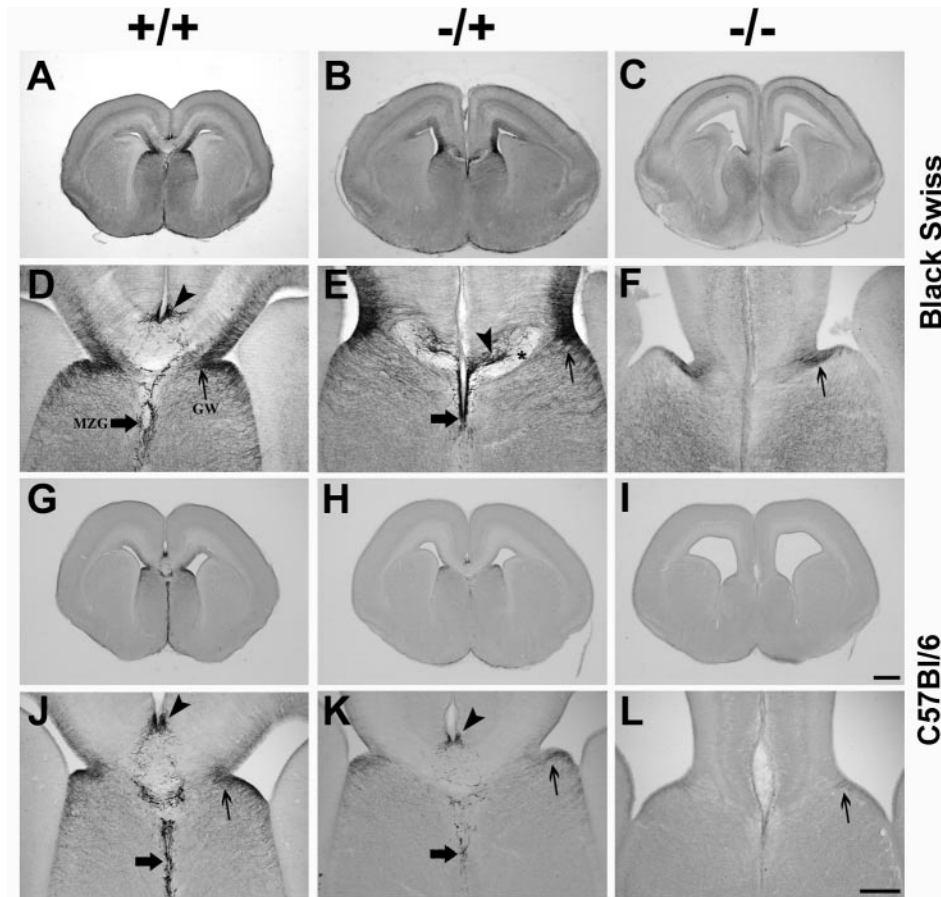
FIG. 6. Midline glial defects in *Nfib*$^{-/-}$ mice. Coronal sections were labeled with an antibody against GFAP to label the midline glial populations. IGG (D, E, J, and K; arrowheads) and MZG (D, E, J, and K; thick arrows) were absent in *Nfib*$^{-/-}$ mice on both the Black Swiss (F) and C57BL/6 (L) backgrounds. The GW was severely reduced in the *Nfib*$^{-/-}$ mice (F and L; thin arrows). Panels D to F and J to L are higher-power views of panels A to C and G to I, respectively. Scale bars, 2 mm (I; applies to panels A to C and G to I) and 200 μm (L; applies to panels D to F and J to L).

TABLE 5. Transcript levels in *Nfib*$^{-/-}$ and *Nfia*$^{-/-}$ brains relative to those in WT brains[a]

Gene	Relative level in:	
	Nfib$^{-/-}$ brain	*Nfia*$^{-/-}$ brain
GFAP	0.2 ± 0.1	0.1 ± 0.01
Tbr2	1.2 ± 0.2	1.9 ± 0.1
Slit2	1.0 ± 0.2	1.0 ± 0.2
Robo1	0.8 ± 0.3	0.8 ± 0.1
Robo2	0.8 ± 0.3	1.3 ± 0.3
Robo3	1.2 ± 0.9	1.5 ± 0.6
DCC	1.1 ± 0.4	1.3 ± 0.1
Sem3A	1.3 ± 0.6	1.5 ± 0.7
Netrin	1.1 ± 0.2	1.6 ± 0.2
Neog	0.9 ± 0.1	1.2 ± 0.3
Neurop1	1.2 ± 0.2	0.8 ± 0.02
Neurop2	1.0 ± 0.3	1.4 ± 0.6
Emx1	1.0 ± 0.1	0.8 ± 0.02
Emx2	1.3 ± 0.2	1.3 ± 0.2
L1	1.1 ± 0.4	0.9 ± 0.1
Sek	1.2 ± 0.5	1.5 ± 0.2
Nuk	1.2 ± 0.3	1.3 ± 0.5

[a] Transcript levels were measured and expressed as described for Table 4.

midline glial populations (11, 56), these data suggest that *Nfia* and *Nfib* may cooperate in the development of these brain regions.

Lung maturation defects in *Nfib*$^{-/-}$ animals. Lung maturation defects that are morphologically similar to those seen in our *Nfib*$^{-/-}$ animals were described previously for an insertion mutation in the *Nfib* locus (22). While that study described the defect as lung hypoplasia, our analysis shows that there is an apparent increase in the amount of DNA in *Nfib*$^{-/-}$ lungs (Table 3), suggesting aberrant cell proliferation and/or apoptosis during lung maturation. Increased PCNA expression at E18.5 in *Nfib*$^{-/-}$ versus WT lungs is also consistent with increased cell proliferation (Table 4). Prenatal lung maturation proceeds through a series of morphologically and biochemically defined stages (10) from budding (approximately E9.5), initial branching morphogenesis and expansion (pseudoglandular, approximately E9.5 to E16.5), continued branching of the distal epithelium and mesenchyme (canalicular; approximately E16.5 to E17.5), and formation of terminal saccules with terminal differentiation of type I and type II epithelial cells (sacculation; approximately E17.5 to P5). Final maturation of the terminal sacs into alveolar ducts and sacs (alveol-
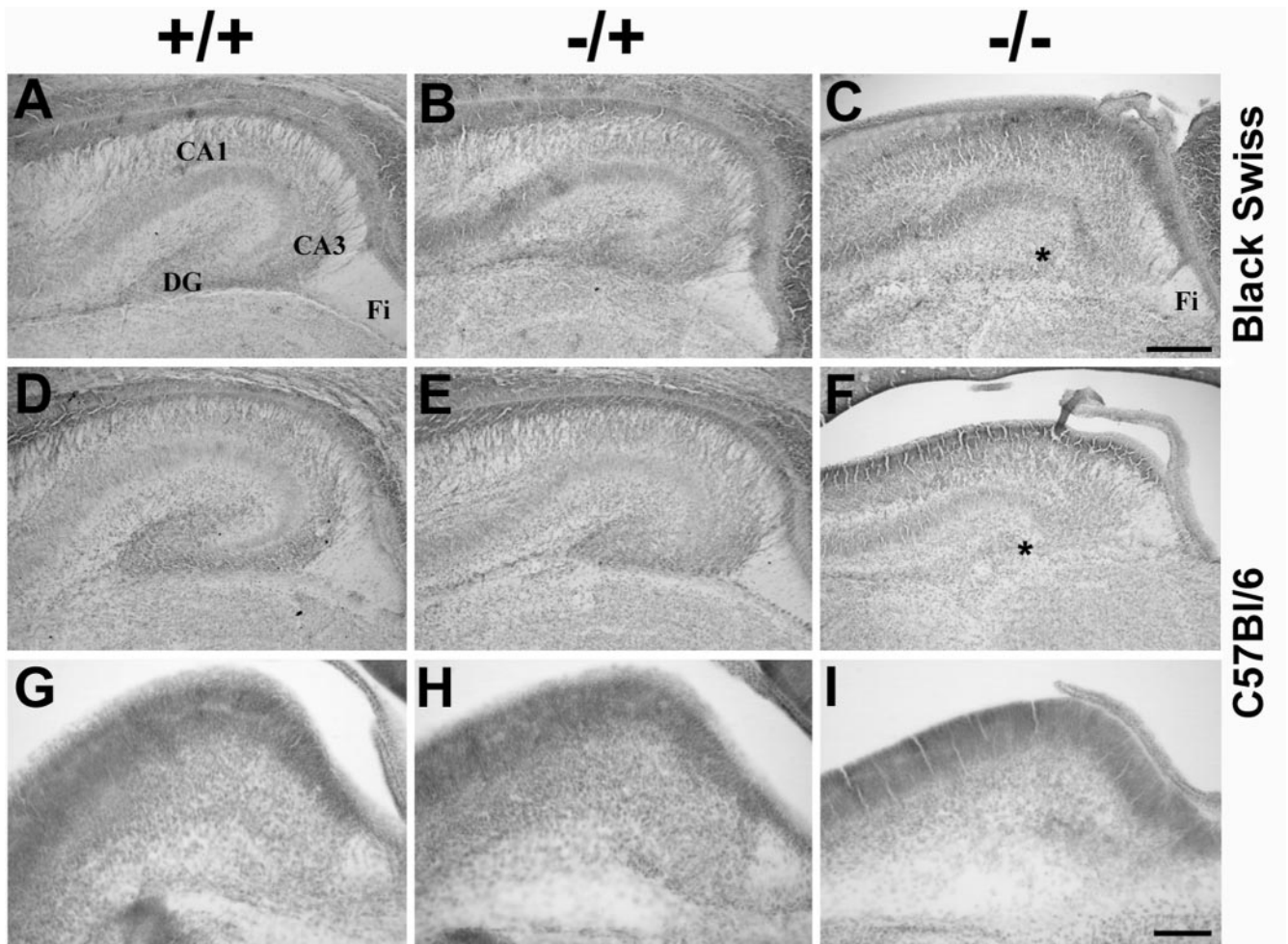
FIG. 7. Development of the hippocampus is severely disrupted in $Nfib^{-/-}$ mice. Coronal 50-μm vibratome sections from E17.5 (A to F) and E15.5 (G to I) embryos were mounted and stained with hematoxylin to reveal the structural morphology of the hippocampus. Gross regionalization of the hippocampus is evident in panel A. Note that the CA2 subfield has not yet developed by E17.5. $Nfib^{-/-}$ mice have a complete absence of the dentate gyrus (DG; asterisks [C and F] denote the region where the DG should have developed) and a reduction in the size of the fimbria (Fi; A and C). (A to C) Sections of brains from mice on a mixed Black Swiss background; (D to I) brains from mice on a C57BL/6 background. Scale bars, 200 μm (C; applies to panels A to F) and 50 μm (I; applies to panels G to I).

ization) occurs postnatally from approximately P5 to P30 (47, 65). The reduction of specific epithelial markers seen here (Table 4), together with the lack of saccule formation, indicates that the lungs in $Nfib^{-/-}$ mice are arrested at the late-pseudoglandular or early-canalicular stage of maturation. Since the morbidity and mortality of premature infants are strongly associated with a failure of lung maturation (45), these mice may provide a useful model to investigate the later stages of prenatal lung maturation.

Failure of late fetal lung maturation has also been seen in mice containing targeted disruptions of the genes encoding glucocorticoid receptor (9), transforming growth factor β3 (55), endothelial nitric oxide synthase (24), and Sp3 (5) and other genes (66, 68, 69). The pathways linking this diverse set of molecules to the developmental events essential for lung maturation have not yet been determined. Given the possible increase in cell number seen in the $Nfib^{-/-}$ lungs (Table 3), it is of interest that the combined loss of p21CIP and p57KIP2, two Cdk inhibitors that mediate cell cycle arrest, results in a

maturation arrest that appears morphologically similar to that seen with loss of $Nfib$ (69). Thus it is possible that $Nfib$ is involved in either mesenchymal or epithelial cell exit from the cell cycle and that this cell cycle arrest is essential for normal maturation of the lung. Consistent with this model are the observations that overexpression of NFIB and other NFI proteins can suppress the oncogenic transformation of chicken embryo fibroblasts mediated by a number of nuclear oncogenes (52) and that rearrangement or altered expression or both of NFIB have been associated with the overgrowth syndromes of pleomorphic adenoma (17) and polycythemia vera (29). To test this model, it will be useful in future studies to determine whether the apparent increase in cell number in the $Nfib^{-/-}$ lungs is due to changes in cell proliferation, apoptosis, or both.

Since $Nfib^{-/-}$ mice have defects in both lung maturation and commissural tract formation (Fig. 2 to 8), it is noteworthy that loss of the known axon guidance receptor gene $Robo1$ also causes perinatal lethality attributed to a failure of lung matu-
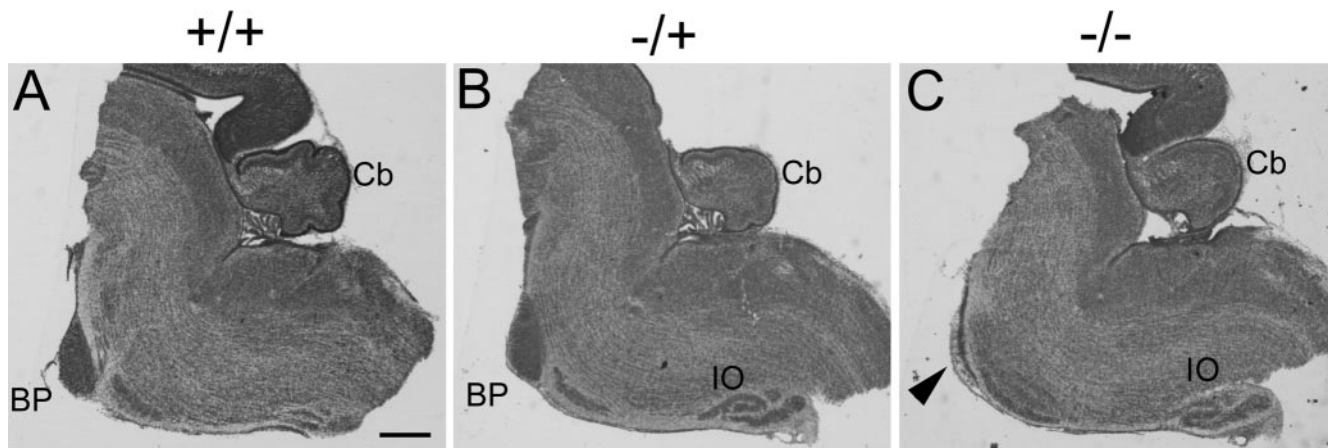
FIG. 8. Absence of the basilar pons in *Nfib*$^{-/-}$ mice. Sagittal sections of E18.5 *Nfib*$^{+/+}$ (A), *Nfib*$^{-/+}$ (B), and *Nfib*$^{-/-}$ (C) hindbrains stained with thionin. Brains were from litters backcrossed for five generations to C57BL/6. The basilar pons (BP) is present in panels A and B but not panel C (arrowhead). The rest of the hindbrain, including the inferior olive (IO), appears normal in the mutant, and the cerebellum (Cb) is present but appears unfoliated in panel C. Scale bar (A), 0.5 mm (applies to all panels).

ration (66). *Robo1* is a mouse ortholog of *Roundabout*, which is essential for normal midline axonal crossing in *Drosophila* (26). The *Robo* gene family encodes receptors with homology to the neural CAM family of cell surface adhesion molecules and appears to regulate axon guidance in both *Drosophila* and mice (49). This gene family has been implicated in regulating axon guidance in mice and humans (27, 37, 63), but its role in lung development is unknown (1). The expression patterns for *Robo* and *Slit* family members during lung maturation are consistent with a role for *Robo* signaling in epithelium-mesenchyme interactions (19). Although we observed no decrease in overall *Robo1* expression in *Nfib*$^{-/-}$ brains (Table 4), analysis of the expression patterns of Robo1 and other signaling molecules by in situ hybridization in *Nfib*$^{-/-}$ animals might reveal regional changes in expression related to the observed phenotypes in brain and lung.

It will be important to determine the specific gene expression changes in *Nfib*$^{-/-}$ lungs that affect maturation. However, given the failure of lung maturation in the *Nfib*$^{-/-}$ mice, it will be essential to distinguish between changes that directly affect the maturation process and those that simply reflect the immature state of the *Nfib*$^{-/-}$ lungs. For example, while we've seen decreases in the expression of a number of type II and type I epithelial markers in E18.5 *Nfib*$^{-/-}$ lungs (Table 4), it is possible these changes merely reflect lack of maturity of the *Nfib*$^{-/-}$ versus *Nfib*$^{+/+}$ lungs. Since the expression levels of

TABLE 6. Levels of the other three *Nfi* genes in *Nfib*$^{-/-}$ lungs and brains[a]

Nfi gene	Relative level in:	
	Nfib$^{-/-}$ E18.5 lungs	*Nfib*$^{-/-}$ E18.5 brains
Nfia	5.1 ± 2.0	2.2 ± 0.6
Nfic	3.3 ± 0.7	1.2 ± 0.4
Nfix	2.8 ± 0.6	1.3 ± 0.3

[a] Transcript levels relative to those in WT organs were assessed by QPCR as described for Table 4.

several of these genes normally increase during lung maturation, it is not surprising that their expression levels are reduced in the less mature *Nfib*$^{-/-}$ lungs. Thus it will be important to determine the earliest time in development at which differences in gene expression between *Nfib*$^{-/-}$ and *Nfib*$^{+/+}$ lungs occur and which of the genes affected at this time are essential for maturation.

One known target for NFI genes in the developing lung epithelium is SP-C. Previous studies showed that the SP-C gene promoter is activated by NFI proteins, including NFI-B2, and that a transgene-encoded dominant repressor (NFI-engrailed) inhibits the expression of SP-C in mouse lung (2, 3). Thus SP-C is a good candidate for a direct target of *Nfib* in the developing lung. However, SP-C is highly expressed only late in lung maturation and SP-C mutant mice do not exhibit a failure in lung maturation (18). Given the expression pattern of the *Nfib::lacZ* allele (Fig. 4), it is possible that *Nfib* regulates both mesenchymal target genes that are essential for the maturation process early in lung development and also epithelial genes that are expressed later in lung development and that are important for physiological functioning of the lung. An important future goal is to distinguish between these two potential classes of *Nfib* target genes.

Neurological defects in *Nfib*$^{-/-}$ animals. While the callosal agenesis (Fig. 5 and 6) and loss of midline GFAP staining (Fig. 6) seen in *Nfib*$^{-/-}$ animals is reminiscent of the phenotype seen previously in *Nfia*$^{-/-}$ mice (11, 56), there are clear morphological differences between the two mutants. For example, *Nfib*$^{-/-}$ animals usually lack large Probst bundles, regions of axonal overlap and swirling near the midline that are often present in *Nfia*$^{-/-}$ animals (56). Such differences imply that, while both genes are essential for callosal formation, they may have both shared and distinct functions in this developmental process. Both *Nfia* and *Nfib* are expressed in the cortex (6, 56) (data not shown), but the lack of markers specific for callosally projecting neurons makes it difficult to assess the significance of this cortical expression. The similar losses of midline glial populations in *Nfib*$^{-/-}$ mice (Fig. 6) and *Nfia*$^{-/-}$ mice (56)

suggest that both genes may cooperate in the growth and differentiation of these midline glial cells. Given the relatively restricted set of glial cells affected by loss of either *Nfia* or *Nfib*, it will be of interest to determine whether simultaneous loss of both *Nfi* genes produces a more severe phenotype in glial cell development.

While both *Nfia*- and *Nfib*-deficient mice exhibit agenesis of the corpus callosum, the *Nfib*-deficient mice have additional neurological defects not reported for *Nfia*-deficient animals, including severe defects in hippocampus (Fig. 7) and pons (Fig. 8) formation. *Nfib* had been shown previously to be expressed in both the hippocampus and the pons (6, 16), and thus it is possible that the defects in these regions are due to cell-autonomous defects in cells that normally express *Nfib*. *Nfib* is one of a small class of genes known to affect hippocampus development, a class which includes the genes *Lhx-5* (70), *Beta2/NeuroD* (34), *Lef-1* (15), *CXCR4* (38), *LRP6* (71), and *Emx-2* (46, 51) and the *Reelin–Disabled-1–beta(1)*-class integrin pathway (14). The mechanisms by which these genes affect the molecular pathways and cellular processes essential for hippocampal development are beginning to be understood. LRP6-deficient mice have generalized defects in the *Wnt*/beta catenin signaling pathway because of the crucial function of LRP6 as a *Wnt* signaling coreceptor (71). These mice have severe defects in the dentate gyrus due to the decreased production of dentate granule cells. They also have abnormalities of the radial glial scaffolding in the forming dentate gyrus. By examining the hippocampal primordium at early stages, the authors showed a reduction in the number of dentate granule cell progenitors in the dentate ventricular zone prior to the emigration of the earliest granule neurons and precursors to form the dentate anlage. It is possible that loss of *Nfib*-regulated gene transcription may lead to a similar alteration of the hippocampal primordium, with resultant severe hypoplasia of the dentate gyrus. A more detailed analysis of early hippocampus development in the *Nfib*$^{-/-}$ mice should allow us to test this model for *Nfib* function in the dentate gyrus.

The molecular mechanisms leading to the loss of the basilar pons in *Nfib*$^{-/-}$ mice are unknown. It may be that *Nfib* regulates one or more signaling molecules, such as DCC or Rig-1/Robo3, that control the migration of pontine neurons to the midline (39). Alternatively, *Nfib* may interact with other transcription factors that regulate pontine formation (4, 13, 33). Distinguishing between these and other possibilities awaits characterization of the fate of pontine neurons in *Nfib*$^{-/-}$ mice. Since analysis of whole-brain RNA has failed to find changes in the expression of some molecules known to influence axon guidance and cell migration (Table 5), determining whether there are common *Nfib* target genes that mediate the defects in callosal formation, hippocampal development, and pons formation will require a detailed analysis of *Nfib* target genes in each of these regions of the brain.

Given the severity of the neurological phenotypes seen in the *Nfib*$^{-/-}$ animals, it is perhaps surprising that a previous study of an insertion of a lacZ translational fusion gene into the *Nfib* locus found no neurological defects (22). This is despite the finding that the lung maturation defects seen in our *Nfib* KO animals appear morphologically similar to those seen in animals with the *Nfib* insertion mutation. There are several possible explanations for such differences. (i) With both our

Nfia$^{-/-}$ and *Nfic*$^{-/-}$ mice we showed that deletion of exon 2 results in aberrant splicing from the first to the third exons of the genes (11, 61). We show a similar aberrant transcript from our disrupted *Nfib* locus (Fig. 1C). These aberrant transcripts do not encode functional proteins as they are missing DNA binding and dimerization domains and as the exons are out of frame, yielding short missense peptides. It is possible that aberrant splicing into the still-present second exon of the insertion mutant gene could generate a hypomorphic, but not null, allele in these animals. In our *Nfib* mutant allele the second exon is deleted, precluding this possibility. (ii) We showed previously that *Nfib* has an alternative first exon, expressed specifically in the brain (21, 42). Splicing from this brain-specific exon into the still present second exon of the insertion mutant gene may be why no brain phenotype for the insertion mutant was seen. Also, the report for the insertion mutant failed to show any β-Gal activity from the targeted allele or to demonstrate loss of *Nfib* expression, making it difficult to compare to the present study. While further studies are needed to resolve these differences, it is clear that our *Nfib*$^{-/-}$ mice have severe lung and brain phenotypes, making them an important tool with which to study *Nfib* function.

NFI gene family in mouse development. Three of the four mouse NFI genes have now been disrupted, and each mutant has unique defects in development. Disruption of *Nfia* results in callosal agenesis, perinatal lethality, hydrocephalus, reduction in the hippocampal commissure, and loss of specific midline glial populations (11, 56). Some of these defects are also present in the *Nfib*$^{-/-}$ mice described here. In contrast, disruption of the *Nfic* gene results in postnatal defects in tooth formation, with no observable defects in neuroanatomy and no lethality if the diet is composed of soft food (61). Since the *Nfib*$^{-/-}$ mice do not survive postnatally, it is not possible to tell if they have tooth defects similar to those seen in *Nfic*$^{-/-}$ mice. Since the four NFI genes encode proteins with highly homologous DNA-binding domains with similar DNA-binding specificities (40), it is possible that there are common downstream targets for all four NFI genes. It is unclear whether the diverse defects seen upon loss of the individual NFI genes are due to differences in the expression patterns of the four genes, differences in downstream target specificity, differences in gene activation or repression by specific NFI isoforms, or other factors. One feature that is common in the mutants is that the defects are seen relatively late in fetal or postnatal development. In *Nfia*$^{-/-}$ and *Nfib*$^{-/-}$ mice the first morphological indication of differences is at E14 to E15, while for *Nfic*$^{-/-}$ mice the first changes are seen at approximately P10. Thus at least three of the four NFI genes are essential for relatively late developmental processes in the mouse. Since the four NFI genes are expressed in an overlapping pattern during development (6) and since changes in NFI transcript levels are first detected at the four-cell stage in embryogenesis (23), it will be of interest to determine whether multiple NFI genes cooperate at earlier stages of mouse development.

It is difficult to connect the diverse defects seen in the *Nfib*$^{-/-}$ mice, callosal agenesis, aberrant gliogenesis, hippocampus and pons development, and failure of lung maturation, into a simple model of *Nfib* function. It will be necessary to determine the earliest stages at which gene expression changes occur in the affected tissues in order to determine

whether common or unique *Nfib* target genes are affected in each organ. Since different NFI proteins have been found to either activate or repress expression from the same promoter depending on the cellular context (7, 8; reviewed in references 21 and 42), it will be important to analyze mice with mutations in multiple NFI genes to determine whether they cooperate or antagonize each other at earlier developmental stages. The future identification of direct downstream targets of *Nfib*, together with analysis of the effects of the combined loss of *Nfib* together with other genes known to affect brain and lung formation, should allow us to determine the molecular mechanisms through which *Nfib* functions in lung and brain development.

REFERENCES

1. **Anselmo, M. A., S. Dalvin, P. Prodhan, K. Komatsuzaki, J. T. Aidlen, J. J. Schnitzer, J. Y. Wu, and T. B. Kinane.** 2003. Slit and robo: expression patterns in lung development. Gene Expr. Patterns **3:**13–19.
2. **Bachurski, C. J., S. E. Kelly, S. W. Glasser, and T. A. Currier.** 1997. Nuclear factor I family members regulate the transcription of surfactant protein-C. J. Biol. Chem. **272:**32759–32766.
3. **Bachurski, C. J., G. H. Yang, T. A. Currier, R. M. Gronostajski, and D. Hong.** 2003. Nuclear factor I/thyroid transcription factor 1 interactions modulate surfactant protein C transcription. Mol. Cell. Biol. **23:**9014–9024.
4. **Ben-Arie, N., B. A. Hassan, N. A. Bermingham, D. M. Malicki, D. Armstrong, M. Matzuk, H. J. Bellen, and H. Y. Zoghbi.** 2000. Functional conservation of atonal and Math1 in the CNS and PNS. Development **127:**1039–1048.
5. **Bouwman, P., H. Gollner, H. P. Elsasser, G. Eckhoff, A. Karis, F. Grosveld, S. Philipsen, and G. Suske.** 2000. Transcription factor Sp3 is essential for post-natal survival and late tooth development. EMBO J. **19:**655–661.
6. **Chaudhry, A. Z., G. E. Lyons, and R. M. Gronostajski.** 1997. Expression patterns of the four nuclear factor I genes during mouse embryogenesis indicate a potential role in development. Dev. Dyn. **208:**313–325.
7. **Chaudhry, A. Z., A. D. Vitullo, and R. M. Gronostajski.** 1998. Nuclear factor I (NFI) isoforms differentially activate simple versus complex NFI-responsive promoters. J. Biol. Chem. **273:**18538–18546.
8. **Chaudhry, A. Z., A. D. Vitullo, and R. M. Gronostajski.** 1999. Nuclear factor I-mediated repression of the mouse mammary tumor virus promoter is abrogated by the coactivators p300/CBP and SRC-1. J. Biol. Chem. **274:**7072–7081.
9. **Cole, T. J., N. M. Solomon, R. Van Driel, J. A. Monk, D. Bird, S. J. Richardson, R. J. Dilley, and S. B. Hooper.** 2004. Altered epithelial cell proportions in the fetal lung of glucocorticoid receptor null mice. Am. J. Respir. Cell Mol. Biol. **30:**613–619.
10. **Costa, R. H., V. V. Kalinichenko, and L. Lim.** 2001. Transcription factors in mouse lung development and function. Am. J. Physiol. Lung Cell. Mol. Physiol. **280:**L823–L838.
11. **das Neves, L., C. Duchala, F. Godinho, M. Haxhiu, C. Colmenares, W. Macklin, C. Campbell, K. Butz, and R. Gronostajski.** 1999. Disruption of the murine nuclear factor I-A gene (*Nfia*) results in perinatal lethality, hydrocephalus and agenesis of the corpus callosum. Proc. Natl. Acad. Sci. USA **96:**11946–11951.
12. **de Jong, R. N., and P. C. van der Vliet.** 1999. Mechanism of DNA replication in eukaryotic cells: cellular host factors stimulating adenovirus DNA replication. Gene **236:**1–12.
13. **Engelkamp, D., P. Rashbass, A. Seawright, and V. van Heyningen.** 1999. Role of Pax6 in development of the cerebellar system. Development **126:**3585–3596.
14. **Forster, E., A. Tielsch, B. Saum, K. H. Weiss, C. Johanssen, D. Graus-Porta,** U. Muller, and M. Frotscher. 2002. Reelin, Disabled 1, and beta 1 integrins are required for the formation of the radial glial scaffold in the hippocampus. Proc. Natl. Acad. Sci. USA **99:**13178–13183.
15. **Galceran, J., E. M. Miyashita-Lin, E. Devaney, J. L. Rubenstein, and R. Grosschedl.** 2000. Hippocampus development and generation of dentate gyrus granule cells is regulated by LEF1. Development **127:**469–482.
16. **Gesemann, M., E. D. Litwack, K. T. Yee, U. Christen, and D. D. O'Leary.** 2001. Identification of candidate genes for controlling development of the basilar pons by differential display PCR. Mol. Cell. Neurosci. **18:**1–12.
17. **Geurts, J. M., E. F. Schoenmakers, E. Roijer, A. K. Astrom, G. Stenman, and W. J. van de Ven.** 1998. Identification of NFIB as recurrent translocation partner gene of HMGIC in pleomorphic adenomas. Oncogene **16:**865–872.
18. **Glasser, S. W., M. S. Burhans, T. R. Korfhagen, C. L. Na, P. D. Sly, G. F. Ross, M. Ikegami, and J. A. Whitsett.** 2001. Altered stability of pulmonary surfactant in SP-C-deficient mice. Proc. Natl. Acad. Sci. USA **98:**6366–6371.
19. **Greenberg, J. M., F. Y. Thompson, S. K. Brooks, J. M. Shannon, and A. L. Akeson.** 2004. Slit and robo expression in the developing mouse lung. Dev. Dyn. **230:**350–360.
20. **Gronostajski, R. M.** 1986. Analysis of nuclear factor I binding to DNA using degenerate oligonucleotides. Nucleic Acids Res. **14:**9117–9132.
21. **Gronostajski, R. M.** 2000. Roles of the NFI/CTF gene family in transcription and development. Gene **249:**31–45.
22. **Grunder, A., T. T. Ebel, M. Mallo, G. Schwarzkopf, T. Shimizu, A. E. Sippel, and H. Schrewe.** 2002. Nuclear factor I-B (*Nfib*) deficient mice have severe lung hypoplasia. Mech. Dev. **112:**69–77.
23. **Hamatani, T., M. G. Carter, A. A. Sharov, and M. S. Ko.** 2004. Dynamics of global gene expression changes during mouse preimplantation development. Dev. Cell **6:**117–131.
24. **Han, R. N., S. Babaei, M. Robb, T. Lee, R. Ridsdale, C. Ackerley, M. Post, and D. J. Stewart.** 2004. Defective lung vascular development and fatal respiratory distress in endothelial NO synthase-deficient mice: a model of alveolar capillary dysplasia? Circ. Res. **94:**1115–1123.
25. **Hogan, B. L., and J. M. Yingling.** 1998. Epithelial/mesenchymal interactions and branching morphogenesis of the lung. Curr. Opin. Genet. Dev. **8:**481–486.
26. **Hummel, T., K. Schimmelpfeng, and C. Klambt.** 1999. Commissure formation in the embryonic CNS of *Drosophila*. Development **126:**771–779.
27. **Jen, J. C., W. M. Chan, T. M. Bosley, J. Wan, J. R. Carr, U. Rub, D. Shattuck, G. Salamon, L. C. Kudo, J. Ou, D. D. Lin, M. A. Salih, T. Kansu, H. Al Dhalaan, Z. Al Zayed, D. B. MacDonald, B. Stigsby, A. Plaitakis, E. K. Dretakis, I. Gottlob, C. Pieh, E. I. Traboulsi, Q. Wang, L. Wang, C. Andrews, K. Yamada, J. L. Demer, S. Karim, J. R. Alger, D. H. Geschwind, T. Deller, N. L. Sicotte, S. F. Nelson, R. W. Baloh, and E. C. Engle.** 2004. Mutations in a human ROBO gene disrupt hindbrain axon pathway crossing and morphogenesis. Science **304:**1509–1513.
28. **Kaplan, F., J. Comber, R. Sladek, T. J. Hudson, L. J. Muglia, T. Macrae, S. Gagnon, M. Asada, J. A. Brewer, and N. B. Sweezey.** 2003. The growth factor midkine is modulated by both glucocorticoid and retinoid in fetal lung development. Am. J. Respir. Cell Mol. Biol. **28:**33–41.
29. **Kralovics, R., Y. Guan, and J. T. Prchal.** 2002. Acquired uniparental disomy of chromosome 9p is a frequent stem cell defect in polycythemia vera. Exp. Hematol. **30:**229–236.
30. **Kruse, U., F. Qian, and A. E. Sippel.** 1991. Identification of a fourth nuclear factor I gene in chicken by cDNA cloning: NFI-X. Nucleic Acids Res. **19:**6641.
31. **Kruse, U., and A. E. Sippel.** 1994. Transcription factor nuclear factor I proteins form stable homo- and heterodimers. FEBS Lett. **348:**46–50.
32. **Labarca, C., and K. Paigen.** 1980. A simple, rapid, and sensitive DNA assay procedure. Anal. Biochem. **102:**344–352.
33. **Li, S., F. Qiu, A. Xu, S. M. Price, and M. Xiang.** 2004. Barhl1 regulates migration and survival of cerebellar granule cells by controlling expression of the neurotrophin-3 gene. J. Neurosci. **24:**3104–3114.
34. **Liu, M., S. J. Pleasure, A. E. Collins, J. L. Noebels, F. J. Naya, M. J. Tsai, and D. H. Lowenstein.** 2000. Loss of BETA2/NeuroD leads to malformation of the dentate gyrus and epilepsy. Proc. Natl. Acad. Sci. USA **97:**865–870.
35. **Livy, D. J., and D. Wahlsten.** 1997. Retarded formation of the hippocampal commissure in embryos from mouse strains lacking a corpus callosum. Hippocampus **7:**2–14.
36. **Livy, D. J., and D. Wahlsten.** 1991. Tests of genetic allelism between four inbred mouse strains with absent corpus callosum. J. Hered. **82:**459–464.
37. **Long, H., C. Sabatier, L. Ma, A. Plump, W. Yuan, D. M. Ornitz, A. Tamada, F. Murakami, C. S. Goodman, and M. Tessier-Lavigne.** 2004. Conserved roles for Slit and Robo proteins in midline commissural axon guidance. Neuron **42:**213–223.
38. **Lu, M., E. A. Grove, and R. J. Miller.** 2002. Abnormal development of the hippocampal dentate gyrus in mice lacking the CXCR4 chemokine receptor. Proc. Natl. Acad. Sci. USA **99:**7090–7095.
39. **Marillat, V., C. Sabatier, V. Failli, E. Matsunaga, C. Sotelo, M. Tessier-Lavigne, and A. Chedotal.** 2004. The slit receptor Rig-1/Robo3 controls midline crossing by hindbrain precerebellar neurons and axons. Neuron **43:**69–79.
40. **Meisterernst, M., I. Gander, L. Rogge, and E. L. Winnacker.** 1988. A quan-

titative analysis of nuclear factor I/DNA interactions. Nucleic Acids Res. **16:**4419–4435.

41. **Mucenski, M. L., S. E. Wert, J. M. Nation, D. E. Loudy, J. Huelsken, W. Birchmeier, E. E. Morrisey, and J. A. Whitsett.** 2003. β-Catenin is required for specification of proximal/distal cell fate during lung morphogenesis. J. Biol. Chem. **278:**40231–40238.

42. **Murtagh, J., F. Martin, and R. M. Gronostajski.** 2003. The nuclear factor I (NFI) gene family in mammary gland development and function. J. Mammary Gland Biol. Neoplasia. **8:**241–254.

43. **Nagata, K., R. Guggenheimer, T. Enomoto, J. Lichy, and J. Hurwitz.** 1982. Adenovirus DNA replication in vitro. Identification of a host factor that stimulates synthesis of the preterminal protein-dCMP complex. Proc. Natl. Acad. Sci. USA **79:**6438–6442.

44. **Nagata, K., R. A. Guggenheimer, and J. Hurwitz.** 1983. Specific binding of a cellular DNA replication protein to the origin of replication of adenovirus DNA. Proc. Natl. Acad. Sci. USA **80:**6177–6181.

45. **National Institutes of Health.** 1994. Report of the Consensus Development Conference on the Effect of Corticosteroids for Fetal Maturation on Perinatal Outcomes. National Institutes of Health, Bethesda Md. http://www.nichd.nih.gov/publications/pubs/corticosteroids/Corticosteroids.html.

46. **Pellegrini, M., A. Mansouri, A. Simeone, E. Boncinelli, and P. Gruss.** 1996. Dentate gyrus formation requires Emx2. Development **122:**3893–3898.

47. **Prodhan, P., and T. B. Kinane.** 2002. Developmental paradigms in terminal lung development. Bioessays **24:**1052–1059.

48. **Reynolds, P. R., M. L. Mucenski, T. D. Le Cras, W. C. Nichols, and J. A. Whitsett.** 2004. Midkine is regulated by hypoxia and causes pulmonary vascular remodeling. J. Biol. Chem. **279:**37124–37132.

49. **Richards, L. J.** 2002. Surrounded by Slit–how forebrain commissural axons can be led astray. Neuron **33:**153–155.

50. **Rupp, R., U. Kruse, G. Multhaup, U. Gobel, K. Beyreuther, and A. Sippel.** 1990. Chicken NFI/TGGCA proteins are encoded by at least three independent genes: NFI-A, NFI-B and NFI-C with homologues in mammalian genomes. Nucleic Acids Res. **18:**2607–2616.

51. **Savaskan, N. E., G. Alvarez-Bolado, R. Glumm, R. Nitsch, T. Skutella, and B. Heimrich.** 2002. Impaired postnatal development of hippocampal neurons and axon projections in the Emx2$^{-/-}$ mutants. J. Neurochem. **83:**1196–1207.

52. **Schuur, E. R., U. Kruse, J. S. Iacovoni, and P. K. Vogt.** 1995. Nuclear factor I interferes with transformation induced by nuclear oncogenes. Cell Growth Differ. **6:**219–227.

53. **Sekine, K., H. Ohuchi, M. Fujiwara, M. Yamasaki, T. Yoshizawa, T. Sato, N. Yagishita, D. Matsui, Y. Koga, N. Itoh, and S. Kato.** 1999. Fgf10 is essential for limb and lung formation. Nat. Genet. **21:**138–141.

54. **Shannon, J. M., and B. A. Hyatt.** 2004. Epithelial-mesenchymal interactions in the developing lung. Annu. Rev. Physiol. **66:**625–645.

55. **Shi, W., N. Heisterkamp, J. Groffen, J. Zhao, D. Warburton, and V. Kaartinen.** 1999. TGF-β3-null mutation does not abrogate fetal lung maturation in vivo by glucocorticoids. Am. J. Physiol. **277:**L1205–L1213.

56. **Shu, T., K. G. Butz, C. Plachez, R. M. Gronostajski, and L. J. Richards.** 2003. Abnormal development of forebrain midline glia and commissural projections in *Nfia* knock-out mice. J. Neurosci. **23:**203–212.

57. **Shu, T., A. C. Puche, and L. J. Richards.** 2003. Development of midline glial populations at the corticoseptal boundary. J. Neurobiol. **57:**81–94.

58. **Shu, T., and L. J. Richards.** 2001. Cortical axon guidance by the glial wedge during the development of the corpus callosum. J. Neurosci. **21:**2749–2758.

59. **Shu, T., V. Sundaresan, M. M. McCarthy, and L. J. Richards.** 2003. Slit2 guides both precrossing and postcrossing callosal axons at the midline in vivo. J. Neurosci. **23:**8176–8184.

60. **Soriano, P., C. Montgomery, R. Geske, and A. Bradley.** 1991. Targeted disruption of the c-src proto-oncogene leads to osteopetrosis in mice. Cell **64:**693–702.

61. **Steele-Perkins, G., K. G. Butz, G. E. Lyons, M. Zeichner-David, H.-J. Kim, M. I. Cho, and R. M. Gronostajski.** 2003. Essential role for NFI-C/CTF transcription-replication factor in tooth root development. Mol. Cell. Biol. **23:**1075–1084.

62. **Stiles, A. D., D. Chrysis, H. W. Jarvis, B. Brighton, and B. M. Moats-Staats.** 2001. Programmed cell death in normal fetal rat lung development. Exp. Lung Res. **27:**569–587.

63. **Sundaresan, V., E. Mambetisaeva, W. Andrews, A. Annan, B. Knoll, G. Tear, and L. Bannister.** 2004. Dynamic expression patterns of Robo (Robo1 and Robo2) in the developing murine central nervous system. J. Comp. Neurol. **468:**467–481.

64. **Tybulewicz, V. L., C. E. Crawford, P. K. Jackson, R. T. Bronson, and R. C. Mulligan.** 1991. Neonatal lethality and lymphopenia in mice with a homozygous disruption of the c-abl proto-oncogene. Cell **65:**1153–1163.

65. **Warburton, D., M. Schwarz, D. Tefft, G. Flores-Delgado, K. D. Anderson, and W. V. Cardoso.** 2000. The molecular basis of lung morphogenesis. Mech. Dev. **92:**55–81.

66. **Xian, J., K. J. Clark, R. Fordham, R. Pannell, T. H. Rabbitts, and P. H. Rabbitts.** 2001. Inadequate lung development and bronchial hyperplasia in mice with a targeted deletion in the Dutt1/Robo1 gene. Proc. Natl. Acad. Sci. USA **98:**15062–15066.

67. **Yagi, T., Y. Ikawa, K. Yoshida, Y. Shigetani, N. Takeda, I. Mabuchi, T. Yamamoto, and S. Aizawa.** 1990. Homologous recombination at c-fyn locus of mouse embryonic stem cells with use of diphtheria toxin A-fragment gene in negative selection. Proc. Natl. Acad. Sci. USA **87:**9918–9922.

68. **Yu, H., A. Wessels, J. Chen, A. L. Phelps, J. Oatis, G. S. Tint, and S. B. Patel.** 2 February 2004, posting date. Late gestational lung hypoplasia in a mouse model of the Smith-Lemli-Opitz syndrome. BMC Dev. Biol. **4:**1. [Online.] http://www.biomedcentral.com/1471-213X/4/1.

69. **Zhang, P., C. Wong, D. Liu, M. Finegold, J. W. Harper, and S. J. Elledge.** 1999. p21(CIP1) and p57(KIP2) control muscle differentiation at the myogenin step. Genes Dev. **13:**213–224.

70. **Zhao, Y., H. Z. Sheng, R. Amini, A. Grinberg, E. Lee, S. Huang, M. Taira, and H. Westphal.** 1999. Control of hippocampal morphogenesis and neuronal differentiation by the LIM homeobox gene Lhx5. Science **284:**1155–1158.

71. **Zhou, C. J., C. Zhao, and S. J. Pleasure.** 2004. Wnt signaling mutants have decreased dentate granule cell production and radial glial scaffolding abnormalities. J. Neurosci. **24:**121–126.